Thin Solid Films 520 (2011) 1136–1140

Contents lists available at SciVerse ScienceDirect

Thin Solid Films

journal homepage: www.elsevier.com/locate/tsf

Low temperature synthesis and electrical characterization of germanium doped Ti-based nanocrystals for nonvolatile memory

Li-Wei Feng [a], Chun-Yen Chang [a], Ting-Chang Chang [b,c,*], Chun-Hao Tu [a], Pai-Syuan Wang [a], Chao-Cheng Lin [d], Min-Chen Chen [b], Hui-Chun Huang [e], Der-Shin Gan [e], New-Jin Ho [e], Shih-Ching Chen [b], Shih-Cheng Chen [f]

[a] *Department of Electronics Engineering & Institute of Electronics, National Chiao Tung University, Hsinchu, 300, Taiwan, ROC*
[b] *Department of Physics, National Sun Yat-Sen University, Kaohsiung, 804, Taiwan, ROC*
[c] *Center for Nanoscience & Nanotechnology, National Sun Yat-Sen University, Kaohsiung, 804, Taiwan, ROC*
[d] *Green Energy and Environment Research Laboratories, Industrial Technology Research Institute, Hsinchu, 310, Taiwan, ROC*
[e] *Institute of Materials Science and Engineering, National Sun Yat-Sen University, Kaohsiung, 804, Taiwan, ROC*
[f] *Department of Electrical Engineering and Institute of Electronic Engineering, National Tsing Hua University, Hsinchu, 310, Taiwan, ROC*

ARTICLE INFO

Article history:
Received 4 March 2010
Received in revised form 7 August 2011
Accepted 9 August 2011
Available online 16 August 2011

Keywords:
Nonvolatile memory
Nanocrystals
Germanosilicide
Titanium
Sputtering
Transmission electron microscopy
X-ray photoelectron microscopy

ABSTRACT

Chemical and electrical characteristics of Ti-based nanocrystals containing germanium, fabricated by annealing the co-sputtered thin film with titanium silicide and germanium targets, were demonstrated for low temperature applications of nonvolatile memory. Formation and composition characteristics of nanocrystals (NCs) at various annealing temperatures were examined by transmission electron microscopy and X-ray photon-emission spectroscopy, respectively. It was observed that the addition of germanium (Ge) significantly reduces the proposed thermal budget necessary for Ti-based NC formation due to the rise of morphological instability and agglomeration properties during annealing. NC structures formed after annealing at 500 °C, and separated well at 600 °C annealing. However, it was also observed that significant thermal desorption of Ge atoms occurs at 600 °C due to the sublimation of formatted GeO phase and results in a serious decrease of memory window. Therefore, an approach to effectively restrain Ge thermal desorption is proposed by encapsulating the Ti-based trapping layer with a thick silicon oxide layer before 600 °C annealing. The electrical characteristics of data retention in the sample with the 600 °C annealing exhibited better performance than the 500 °C-annealed sample, a result associated with the better separation and better crystallization of the NC structures.

© 2011 Elsevier B.V. All rights reserved.

1. Introduction

Compared to conventional floating-gate nonvolatile memory (NVM) devices, NVMs with metal nanocrystals (NCs) as the floating storage node have received much attention due to their higher energy state density, stronger coupling with the device channel, wider range of available work functions, and stronger charge confinement [1–3]. They can be applied as ultralow-power and high-density memories with long retention time, due to strong quantum confinement of charges in the NCs. Among them, titanium (Ti)-based NCs, such as titanium nitride (TiN) and titanium oxide (TiO_2) [4–7], are excellent for NVM applications due to their advantages of easy fabrication, low cost, good heat stability, and excellent compatibility with complementary metal-oxide-semiconductor processes. However, reports indicate that a fabrication temperature higher than 900 °C is necessary to exhibit NVM characteristics. Such a high temperature process is not suitable for low temperature process applications such as fabrication on a glass substrate. According to the research, however, the presence of germanium (Ge) in Ti silicide film affects not only the phase formation temperature but also its morphological stability, meaning that a low-resistance Ti germanosilicide phase can be formed at a lower temperature than Ti silicide [8]. In addition, poor morphological stability could be obtained by a lowering of agglomeration temperature of Ti silicide with Ge [9–11]. So, incorporation of Ge into titanium silicide seems to allow for the formation of Ti-based NCs at a relatively low fabrication temperature. In this study, therefore, we research the temperature dependence of formation of Ti-based NCs with Ge composition as well as the chemical and electrical characteristics for NVM applications.

2. Experiment

After a standard RCA clean process for a p-type silicon (100) wafer, a 4-nm-thick thermal oxidation layer was grown as the tunneling

* Corresponding author at: Department of Physics, National Sun Yat-Sen University, Kaohsiung, 804, Taiwan, ROC
E-mail address: tcchang@mail.phys.nsysu.edu.tw (T.-C. Chang).

0040-6090/$ – see front matter © 2011 Elsevier B.V. All rights reserved.
doi:10.1016/j.tsf.2011.08.025

oxide layer. Then, an ~10-nm-thick Ti-based germanosilicide layer was deposited to act as a charge trapping layer by co-sputtering $TiSi_2$ and Ge targets in Argon ambient at a pressure of 1 Pa. The applied direct currents on $TiSi_2$ and Ge targets were fixed at 100 W and 50 W, respectively. Next, a thin silicon dioxide layer of 10 nm was deposited by plasma enhanced chemical vapor deposition before annealing treatments (denoted as "10 nm-pre-capped sample") in order to reduce a possible contamination of the trapping layer during atmospheric exposure. For comparison, another sample set with a thicker pre-capped oxide of 20 nm (denoted as "20 nm-pre-capped sample") was also prepared in order to further discuss thermal desorption phenomena of the charge trapping layer during the subsequent annealing process. After encapsulation of the thin oxide layers, a rapid temperature annealing (RTA) was carried out at different temperature conditions of 400 °C, 500 °C and 600 °C for 2 min to compare the temperature-related formation characteristics of NCs. After the annealing treatments, once again a 30-nm-thick and a 20-nm-thick silicon oxide layer were deposited on the 10 nm-pre-capped and 20 nm-pre-capped samples, respectively. The 40 nm-thick oxide layer, including the pre-capped oxide, was produced to act as the blocking oxide. Finally, a 500-nm-thick Al gate electrode was deposited and patterned by shadow mask to form a capacitor structure for electrical measurements. The control samples without Ge composition in the charge trapping layer, i.e., only a 10-nm-thick $TiSi_2$ as the trapping layer, were also fabricated with the same process conditions for comparison. The microstructure and chemical material analyses were conducted by transmission electron microscopy (TEM) and X-ray photoelectron spectroscopy (XPS), respectively. Cross-sectioned TEM samples were prepared using the focused ion beam system (FIB, SEIKO SMI3050SE; ion beam operating at 30 kV and 200–7000 pA) lift-out method and were analyzed by a Philips Tecnai-20 System operating at an accelerating voltage of 200 kV. The sample thickness was about 80 nm. XPS was prepared using a PHI Quantera SXM/Auger AES 650 spectrometer with a monochromatized Al Kα X-ray source (1486.6 eV; 300 W) with a background pressure of 3×10^{-8} Pa by spherical capacitor analyzer and was adopted from the annealed samples only after the pre-capped oxide deposition. Besides, an ion beam is used to erode the sample surface for destructive depth profiling analysis. XPS fitting is by using XPSPEAK41 tool. The ion sputtering energy used for the XPS depth profiling is 5 keV on the SiO_2 layer till the appearance of higher Ti and Ge signals. In addition, capacitance–voltage (C–V) hysteresis and electrical retention characteristics were performed by a HP4284 Precision LCR Meter with high frequency of 1 MHz.

3. Results and discussion

Fig. 1 shows cross-sectional TEM of the 10-nm-pre-capped samples with the annealing treatments of (a) 400 °C, (b) 500 °C, and (c) 600 °C as well as the 20-nm-pre-capped sample with the annealing treatment of (d) 600 °C. It can be observed that a blanket Ti-based germanosilicide film was still maintained even after the 400 °C annealing, as shown in Fig. 1 (a). However, after the 500 °C annealing, the Ti-based germanosilicide film began to agglomerate and form incomplete NC structures, as shown in Fig. 1(b). After the 600 °C annealing, well-separated NCs structures were obtained, as shown in Fig. 1(c) and (d). Comparison of Fig. 1(c) and (d) with the same annealing conditions shows an expansion of the NC size as well as a decrease of the NC/SiO_2 contrast that was evident in the 10-nm-pre-capped sample [Fig. 1(c)]. These phenomena could be due to ineffective protection of the Ti-based germanosilicide layer against Ge thermal desorption, which was confirmed by the XPS results discussed below. In contrast, the 20-nm-pre-capped sample was observed to exhibit better crystallization due to the existence of Ge to reduce the phase formation temperature. The diffraction pattern of the NCs was analyzed by Fourier transformation with the Gatan tool, as shown in Fig. 1(d), because the crystallization characteristics of the materials, the small dimensions of the NCs, and the influence of material surrounding the NCs act to limit the experimental analysis of the diffraction pattern. As shown in the inset of Fig. 1(d), a cubic structure was calculated, indicating the [011]Ge structure, as shown below; therefore, Si – Ge precipitates could be assumed to occur in the sample.

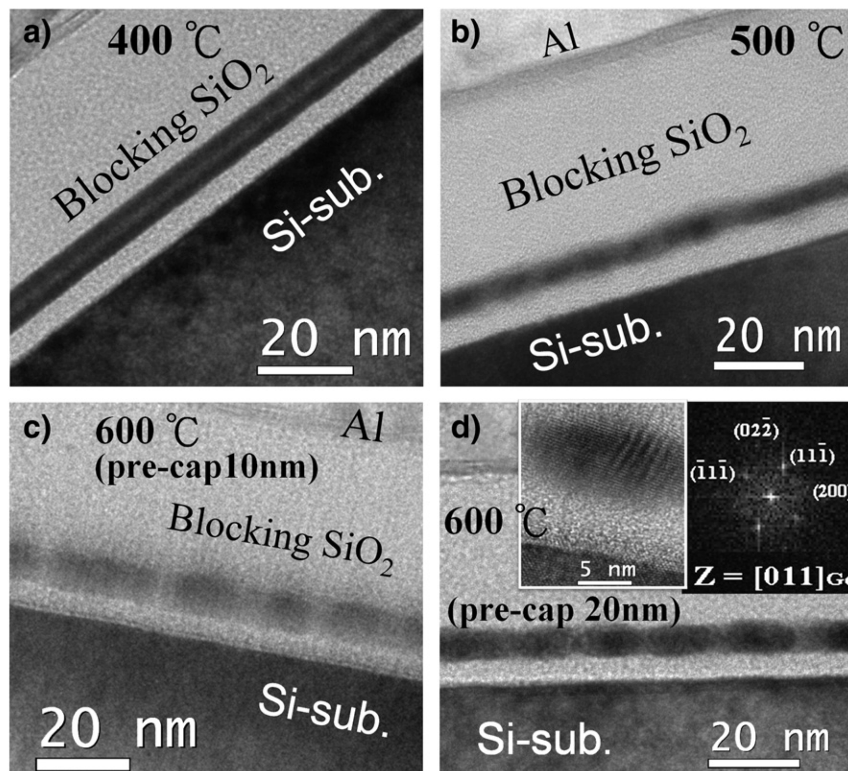

Fig. 1. Cross-sectional TEM of the 10-nm-pre-capped samples with annealing treatments of (a) 400 °C, (b) 500 °C, and (c) 600 °C as well as the 20-nm-pre-capped sample with annealing treatment of (d) 600 °C. The inset of Fig. 1(d) shows Fourier transformation with Gatan tool of the NCs in Fig. 1(d).

Fig. 2(a), (b), and (c) shows XPS spectra of the 10-nm-pre-capped samples with different annealing conditions for O-*1s*, Si-*2p*, and Ti-*2p*, respectively. All the XPS data were adopted from only the annealed samples with the pre-capped oxide layer after argon milling of the pre-capped oxide. The O-*1s* spectrum [Fig. 2(a)] shows that the main peak signal for Si – O bonding [12] is intact in the samples annealed at 400 °C, and 500 °C, and shifts toward higher binding energy in the sample annealed at 600 °C, representing more complete Si – O bonding [13]. This could be attributed to the formation of more stoichiometric and more condensed silicon oxide separated from the trapping layer due to the agglomeration of Ti-based germanosilicide NCs after high temperature treatment. In the Si-*2p* spectrum [Fig. 2 (b)], a peak signal at 102.7 eV related to Si – O [14] bonding was observed in the sample annealed at 400 °C. Additionally, another peak signal at 99.6 eV, corresponding to Si – Si binding [15], appears in the sample annealed at 500 °C and increases slightly in the sample annealed at 600 °C. In addition, the Si – O peak also shifts toward a higher binding energy of 103.1 eV after the 600 °C annealing, consistent with O-*1s* due to more complete Si – O bonding. In the Ti-*2p* spectrum of Fig. 2(c), Ti – O peak signals referenced as TiO_2 [16] were detected after all annealing conditions. The Ti atom is easily oxidized since TiO_2 is a thermodynamically stable phase, and hence, the trace O_2 in RTA ambient or the absorbed O_2 on the wafer surface during wafer transportation (air exposure) is enough to produce Ti – O bonding during high temperature annealing [17–19]. In addition, after the 500 °C and 600 °C annealing, one more peak, representing Ti – O – Si bonding, was observed [20]. Of note, we have also checked the XPS spectra around 454 eV and no signal peaks were observed near this range. Moreover, no peak appears around 99 eV in Fig. 2 (b) at 400 °C. Therefore, these results show the disappearance of the $TiSi_2$ peak. This suggests that the Ti atom is easily oxidized since TiO_2 is a thermodynamically stable phase, i.e., Ti atoms prefer to bond to O atoms instead of Si atoms. In the Ge-2*p* spectra [Fig. 2(d)], it was observed that not only a Ge peak signal but also considerable GeO, and GeO_2 peak signals were apparent in the sample annealed at 400 °C, similar to Ti atoms and contributing to the ease of oxidation of Ge atoms in the presence of O_2 ambient [16]. After the 500 °C annealing, Ge – Ge binding dominates rather than the Ge – O bindings. According to the XPS results for Si and Ge signals, the appearance of Si – Si and Ge – Ge bonds could be related to the formation of Si – Ge [21] and is contributed by the Si – Ge precipitates [22,23]. Moreover, since the enthalpy of $TiSi_2$ formation is larger than that of $TiGe_2$ [13,24], there is a tendency for Si to replace Ge in Ti – Si – Ge compounds [25]. Such a replacement accompanies the formation of germanium-rich Si – Ge precipitates, causing the remarkable Ge – Ge signals. Note that peak signals related to elemental Ge were only clearly observed in the 10-nm-pre-capped samples after the 400 °C and 500 °C annealing, but severely decreased after the 600 °C annealing. Since the XPS data were collected from the annealed samples only with the pre-capped oxide layer after argon milling of the pre-capped oxide, the major impact to the XPS data could be the variation of the argon milling rate, which would cause difficulty in collecting data at the same depth of the trapping layer, i.e., the elemental intensities analyzed from different samples are hard to compare. However, the XPS data are still useful to compare the relative intensity by referencing the different elemental intensities from the same sample. The atomic concentration ratio of Ge-*2p*/Ti-*2p* was examined

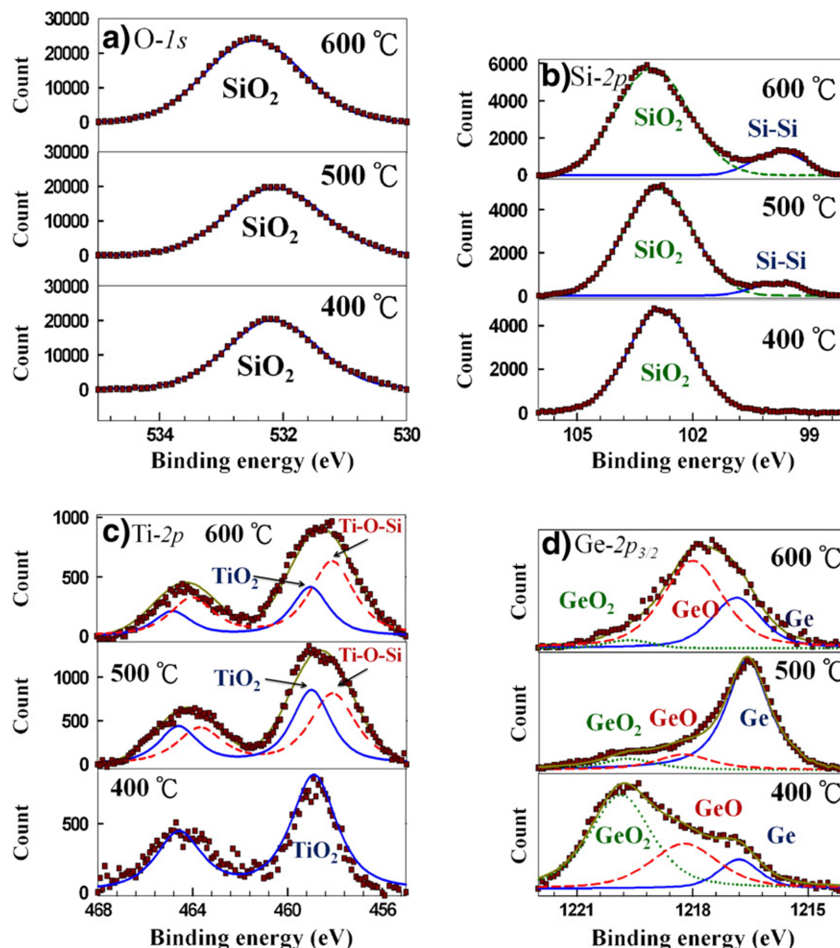

Fig. 2. XPS spectra of the 10-nm-pre-capped samples with the annealing conditions of 400 °C, 500 °C, and 600 °C for (a) O-1*s*, (b) Si-2*p*, and (c) Ti-2*p* as well as the 20-nm-pre-capped sample for (d) Ge-2*p*.

separately in the two samples via quantitative XPS analysis for comparison. The atomic concentration ratio of Ge-*2p*/Ti-*2p* clearly reduced from 3.62 in the 500 °C-annealed sample to 0.41 in the 600 °C-annealed sample, consistent with the TEM contrast results discussed above. In order to further confirm the binding characteristics at the 600 °C-treated condition, an analysis of the Ge-*2p* XPS spectra was also carried out on the 20-nm-pre-capped sample. A large amount of non-stoichiometric germanium oxide was observed in the 20-nm-pre-capped sample after the 600 °C annealing. The existence of GeO might be caused from oxidation of the precipitated Ge during the 600 °C-annealing process. In addition, it has been reported that the GeO phase is too thermodynamically unstable at such annealing conditions, so sublimes [26,27]. Therefore, occurrence of a severe decrease of Ge in the 10-nm-pre-capped sample after the 600 °C annealing can be indirectly confirmed as thermal desorption due to sublimation of the GeO formation phase. According to the XPS results, therefore, the NC charge trapping layer was mainly composed of titania-germanosilicide after the 500 °C annealing and mainly titania-germanium oxide after the 600 °C annealing.

Fig. 3 shows a comparison of high frequency C–V characteristics on the 10-nm-pre-capped samples with annealing treatments of (a) 400 °C, (b) 500 °C, and (c) 600 °C. As shown in Fig. 3(a), nearly no flat band voltage shift (ΔV_{th}) was observed with gate bias voltage sweeping in the sample after the 400 °C annealing, mainly due to the continuous structure of the charge trapping layer. When the annealing temperature was increased to 500 °C [Fig. 3(b)], large ΔV_{th} of ~1.8 V, ~4 V, and ~6.1 V were obtained while the gate voltage was swept in the range between 3/−3 V, 5/−5 V, and 7/−7 V, respectively. In addition, the observed counterclockwise hysteresis loops indicate that charge carriers were injected from the silicon substrate through the tunnel oxide. However, when the 600 °C annealing condition was performed, the ΔV_{th} reduced significantly, as shown in Fig. 3(c). By contrast, Fig. 3 (d) also shows C–V characteristics of the 20-nm-pre-capped sample after the 600 °C annealing. Again, ΔV_{th} of ~0.6 V, ~1.2 V, and ~3.8 V were observed under the gate voltage sweeping ranges of 3/−3 V, 5/−5 V, and 7/−7 V, respectively. On the other hand, the control samples, whose charge trapping layer was composed of only $TiSi_2$, show no flat band voltage shifts after the 400 °C, 500 °C or 600 °C annealing conditions (not shown here). Additionally, Ge NCs reported in past research for NVMs applications [28–30] were almost all fabricated above such temperatures. According to the discussions above, therefore, we suggest that memory effects are strongly influenced by the addition of Ge in Ti-based NCs instead of only Ge or TiO_2 NCs.

Fig. 4 shows a comparison of retention characteristics between the 10-nm-pre-capped sample annealed at 500 °C and the 20-nm-pre-capped one annealed at 600 °C. After both devices were operated to a condition having nearly the same memory window of ~3.5 V, the memory windows of the 10 nm-capped sample and the 20 nm-capped sample still retained ~1.30 V and ~1.75 V after 10^4 s, respectively. Better retention characteristics were found in the sample with a higher temperature treatment, indicating better separation of the charge storage NCs.

4. Conclusion

In conclusion, the memory effects of Ti-based NCs fabricated by annealing co-sputtered thin film with titanium silicide and germanium targets were demonstrated at a relatively low fabrication temperature of 500 °C, necessary due to the presence of Ge atoms. However, as the annealing temperature was increased to 600 °C, thermal desorption of Ge atoms occurred and severely degraded the electrical characteristics of the threshold voltage shift. An effective approach to suppressing such a thermal desorption at 600 °C was proposed by depositing an efficient pre-capped oxide layer (20 nm here) on the trapping layer before

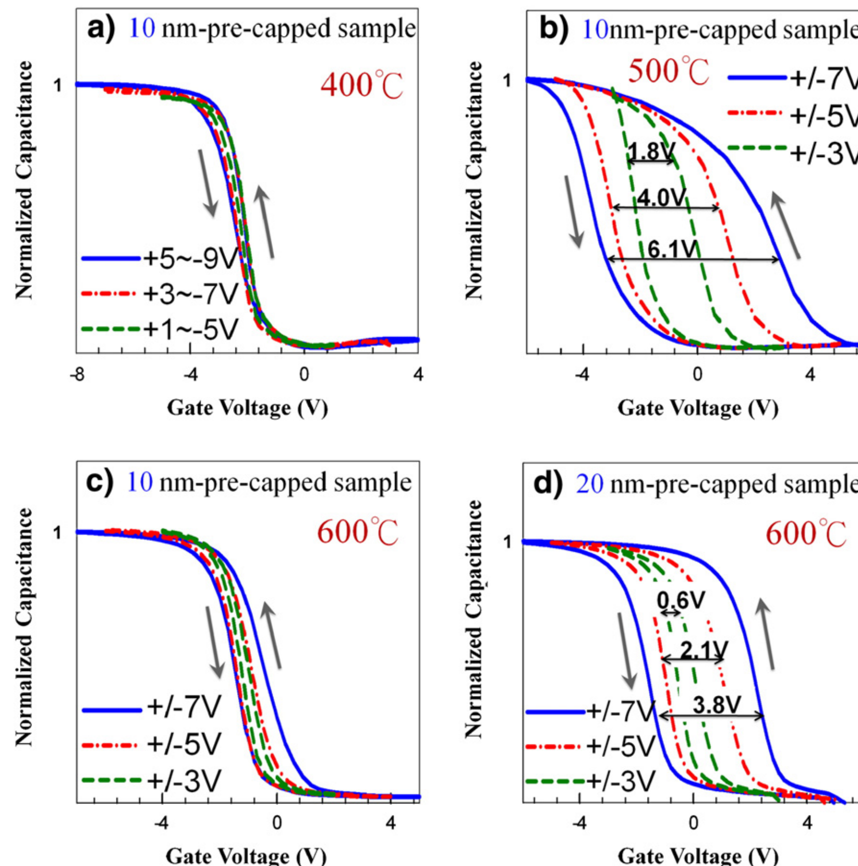

Fig. 3. A comparison of high frequency C–V characteristics on the 10-nm-pre-capped samples with annealing treatment of (a) 400 °C, (b) 500 °C, and (c) 600 °C as well as the 20-nm-pre-capped sample with annealing treatment of (d) 600 °C.

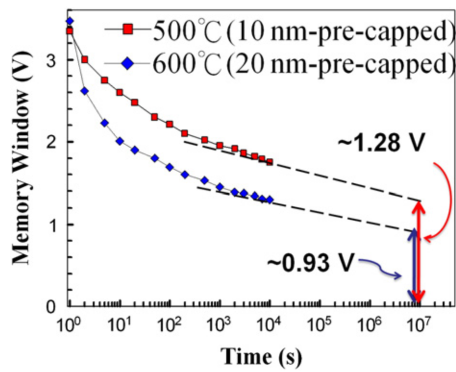

Fig. 4. A comparison of retention characteristics between the 10-nm-pre-capped sample annealed at 500 °C and the 20-nm-pre-capped one annealed at 600 °C.

annealing treatments. By annealing the efficiently encapsulated NVM device at 600 °C, better crystallization and separation of the Ti-based NCs can be obtained and results in better electrical retention performance when compared to the 500 °C-annealed one.

This work was performed at National Nano Device Laboratory and was supported by the National Science Council of the Republic of China under Contract nos. NSC 96-2221-E-009-202-MY3, NSC 97-2112-M-110-009-MY3, and no. NSC 98-3114-M-110-001.

References

[1] T.C. Chang, P.T. Liu, S.T. Yan, S.M. Sze, Electrochem. Solid-State Lett. 8 (2005) G71.
[2] T.C. Chang, S.T. Yan, C.H. Hsu, M.T. Tang, J.F. Lee, Y.H. Tai, P.T. Liu, S.M. Sze, Appl. Phys. Lett. 84 (2004) 2581.
[3] P.H. Yeh, C.H. Yu, L.J. Chen, H.H. Wu, P.T. Liu, T.C. Chang, Appl. Phys. Lett. 87 (2005) 193504.
[4] S.O. choi, S.S. Kim, M. Chang, H.S. Hwang, S.H. Jeon, C.W. Kim, Appl. Phys. Lett. 86 (2005) 123110.
[5] S. Mailap, P.J. Tzeng, H.Y. Lee, C.C. Wang, T.C. Tien, L.S. Lee, M.J. Tsai, Appl. Phys. Lett. 91 (2007) 043114.
[6] C.H. Lin, C.C. Wang, P.J. Tzeng, Maikap Siddheswar, H.Y. Lee, L.S. Lee, M.J. Tsai, Jpn. J. Appl. Phys. 46 (4B) (2007) 2523.
[7] L.W. Feng, C.Y. Chang, T.C. Chang, C.H. Tu, P.S. Wang, Y.F. Chang, M.C. Chen, H.C. Huang, Appl. Phys. Lett. 95 (2009) 262110.
[8] B. Umapathi, S. Das, S.K. Lahiri, S. Kal, J. Electron. Mater. 30 (2001) 17.
[9] D.B. Aldrich, Y.L. Chen, D.E. Sayers, R.J. Nemanich, S.P. Ashburn, M.C. Ozturk, J. Appl. Phys. 77 (1995) 5107.
[10] N. Boutarek, R. Madar, Appl. Surf. Sci. 73 (1993) 209.
[11] O. Thomas, F.M. d'Heurle, S. Delage, J. Mater. Res. 5 (1990) 1453.
[12] I. Bertoti, G. Varsanyi, G. Mink, T. Szekely, J. Vaivads, T. Millers, J. Grabis, Surf. Interface Anal. 12 (1988) 527.
[13] R. Alfonsetti, G. De Simone, L. Lozzi, M. Passacantando, P. Picozzi, S. Santucci, Surf. Interface Anal. 22 (1994) 89.
[14] L.P. Chen, Y.C. Chan, S.J. Chang, G.W. Huang, C.Y. Chang, Jpn. J. Appl. Phys. 37 (1998) L 122.
[15] J. Finster, Surf. Interface Anal. 12 (1988) 309.
[16] H. Noda, K. Oikawa, T. Ogata, K. Matsuki, H. Kamada, Chem. Soc. Jpn. 8 (1986) 1084.
[17] C.H. Lin, C.C. Wang, P.J. Tzeng, S. Maikap, H.Y. Lee, L.S. Lee, M.J. Tsai, Jpn. J. Appl. Phys. Part 1 46 (2007) 2523.
[18] C.H. Lin, C.C. Wang, P.J. Tzeng, C.S. Liang, W.M. Lo, H.Y. Li, L.S. Lee, S.C. Lo, Y.W. Chou, M.J. Tsai, Jpn. J. Appl. Phys. 45 (2006) 3036.
[19] J.M. Wang, W.G. Liu, T. Mei, Ceram. Int. 30 (2004) 1921.
[20] W.X. Xu, Shu Zhu, X.C. Fu, Appl. Surf. Sci. 136 (1998) 194.
[21] Y.D. Zheng, R. Zhang, L.Q. Hu, S.Y. Mo, X.N. Li, P.X. Zhong, Phys. Scr. 41 (1990) 104.
[22] D.B. Aldrich, F.M. d'Heurle, D.E. Sayers, R.J. Nemanich, Phys. Rev. B 53 (1996) 16279.
[23] W.R. Chen, T.C. Chang, P.T. Liu, C.H. Tu, J.L. Yeh, Y.T. Hsieh, R.Y. Wang, C.Y. Chang, Surf. Coat. Technol. 202 (2007) 1333.
[24] F.R. deBoer, R. Boom, W.C.M. Mattens, A.R. Miedema, A.K. Niessen, Cohes. Met. Transit. Met. Alloys North-Hollan, Amsterdam 1 (1988) 127.
[25] James E. Burnette, Robert J. Nemanich, Dale E. Sayers, J. Appl. Phys. 97 (2005) 113521.
[26] Y. Pauleau, J.C. Remy, J. Less-Common Met. 42 (1975) 199.
[27] Oh. Jungwoo, Joe C. Campbell, J. Electron. Mater. 33 (2004) 364.
[28] X.B. Lu, P.F. Lee, J.Y. Dai, Appl. Phys. Lett. 86 (2005) 203111.
[29] S. Duguay, J.J. Grob, A. Slaoui, Y. Le Gall, M. Amann-Liess, J. Appl. Phys. 97 (2005) 104330.
[30] T.H. Ng, W.K. Chim, W.K. Choi, V. Ho, L.W. Teo, A.Y. Du, C.H. Tung, Appl. Phys. Lett. 84 (2004) 4385.